Inorganic Chemistry
Article

Inorg. Chem. **2010**, *49*, 1801–1810 **1801**
DOI: 10.1021/ic902189g

Electronic Structures of Pd^{II} Dimers

John E. Bercaw,[†] Alec C. Durrell,[†] Harry B. Gray,*[,†] Jennifer C. Green,*[,‡] Nilay Hazari,[†,§] Jay A. Labinger,*[,†] and Jay R. Winkler[†]

[†]*Arnold and Mabel Beckman Laboratories of Chemical Synthesis, California Institute of Technology, Pasadena, California 91125, and* [‡]*Department of Chemistry, Oxford University, Inorganic Chemistry Laboratory, South Parks Road, Oxford OX1 3QR, United Kingdom.* [§]*Present address: Chemistry Department, Yale University, P.O. Box 208107, New Haven, Connecticut 06520.*

Received November 5, 2009

The Pd^{II} dimers [(2-phenylpyridine)Pd(μ-X)]$_2$ and [(2-*p*-tolylpyridine)Pd(μ-X)]$_2$ (X = OAc or TFA) do not exhibit the expected planar geometry (of approximate D_{2h} symmetry) but instead resemble an open "clamshell" in which the acetate ligands are perpendicular to the plane containing the Pd atoms and 2-arylpyridine ligands, with the Pd atoms brought quite close to one another (approximate distance 2.85 Å). The molecules adopt this unusual geometry in part because of a d^8-d^8 bonding interaction between the two Pd centers. The Pd−Pd dimers exhibit two successive one-electron oxidations: $Pd^{II}-Pd^{II}$ to $Pd^{II}-Pd^{III}$ to $Pd^{III}-Pd^{III}$. Photophysical measurements reveal clear differences in the UV−visible and low-temperature fluorescence spectra between the clamshell dimers and related planar dimeric [(2-phenylpyridine)Pd(μ-Cl)]$_2$ and monomeric [(2-phenylpyridine)Pd(en)][Cl] (en = ethylenediamine) complexes that do not have any close Pd−Pd contacts. Density functional theory and atoms in molecules analyses confirm the presence of a Pd−Pd bonding interaction in [(2-phenylpyridine)Pd(μ-X)]$_2$ and show that the highest occupied molecular orbital is a d_{z^2} σ^* Pd−Pd antibonding orbital, while the lowest unoccupied molecular orbital and close-lying empty orbitals are mainly located on the 2-phenylpyridine rings. Computational analyses of other $Pd^{II}-Pd^{II}$ dimers that have short Pd−Pd distances yield an orbital ordering similar to that of [(2-phenylpyridine)Pd(μ-X)]$_2$, but quite different from that found for d^8-d^8 dimers of Rh, Ir, and Pt. This difference in orbital ordering arises because of the unusually large energy gap between the 4d and 5p orbitals in Pd and may explain why Pd d^8-d^8 dimers do not exhibit the distinctive photophysical properties of related Rh, Ir, and Pt species.

Introduction

Complexes containing metal−metal bonds play an important role in both inorganic and organometallic chemistry.[1] Among the many such complexes, dimers of square planar Rh^{I}, Ir^{I}, and Pt^{II} centers are members of a special class that feature attractive d^8-d^8 interactions, as documented by optical and vibrational spectroscopy,[2] X-ray crystallography,[3] extended X-ray absorption fine structure,[4] and ab initio electronic structure theory.[5] Overlap in the axial direction between the valence d_{z^2} orbitals of the square planar metal centers results in both filled bonding (dσ) and antibonding (dσ*) orbitals; however, there is a net overall bonding interaction due to symmetry-allowed mixing with the $(n+1)$ metal s and p_z orbitals. This creates four key orbitals (labeled according to their principal atomic character) in the following order of increasing energy: one strongly bonding (dσ), one weakly antibonding (dσ*), one weakly bonding (pσ), and one strongly antibonding (pσ*); only the first two are filled (Figure 1). Such d^8-d^8 interactions most commonly lead to discrete dimers or trimers, although in some cases higher-order oligomers are formed.

In 1975, Mann et al. reported the electronic spectroscopic characterization of $[Rh(CNPh)_4]_n^{n+}$ (n = 1, 2, or 3) in acetonitrile solution and proposed that aggregation occurred through a direct Rh−Rh interaction.[2a] Since this initial discovery, many d^8-d^8 dimers of Rh^{I}, Ir^{I}, and Pt^{II} have been

*To whom correspondence should be addressed. E-mail: hbgray@caltech.edu(H.B.G.), jennifer.green@chem.ox.ac.uk (J.C.G.), jal@caltech.edu (J.A.L.).

(1) (a) Cotton, F. A. *Inorg. Chem.* **1998**, *37*, 5710. (b) Cotton, F. A.; Murillo, C. A.; Bochmann, M. *Advanced Inorganic Chemistry*, 6th ed.; John Wiley & Sons: New York, 1999; pp 647−652.

(2) (a) Mann, K. R.; Gordon, J. G.; Gray, H. B. *J. Am. Chem. Soc.* **1975**, *97*, 3553. (b) Mann, K. R.; Gray, H. B. *Adv. Chem. Ser.* **1979**, *173*, 225. (c) Rice, S. F.; Milder, S. J.; Goldbeck, R. A.; Kliger, D. S.; Gray, H. B. *Coord. Chem. Rev.* **1982**, *43*, 349.

(3) (a) Osborn, R. S.; Rogers, D. *J. Chem. Soc., Dalton Trans.* **1974**, 1002. (b) Connick, W. B.; Marsh, R. E.; Schaefer, W. P.; Gray, H. B. *Inorg. Chem.* **1997**, *36*, 913.

(4) Carr, N.; Crossley, J. G.; Dent, A. J.; Gouge, J. R.; Greaves, G. N.; Jarrett, P. S.; Orpen, A. G. *J. Chem. Soc., Chem. Commun.* **1990**, 11369.

(5) (a) Novoa, J. J.; Aullon, G.; Alemany, P.; Alvarez, S. *J. Am. Chem. Soc.* **1995**, *117*, 7169. (b) Aullón, G.; Alvarez, S. *Chem.—Eur. J.* **1997**, *3*, 655.

Published on Web 01/21/2010

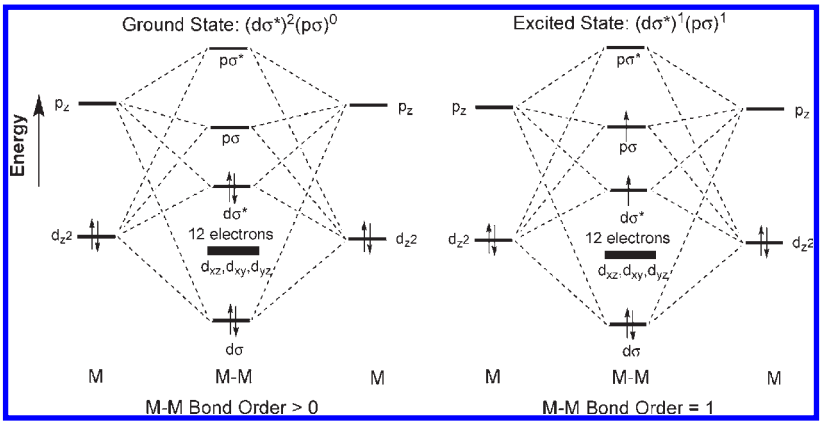

Figure 1. Orbital energy level diagram for interaction along the metal−metal axis of two d^8 square-planar units, in both ground and excited states.

found to exhibit a rich diversity of reactions resulting from photoexcitation and the accompanying increase in metal−metal bond order (Figure 1). A particularly widely studied d^8-d^8 dimer is $Pt_2(\mu\text{-}P_2O_5H_2)_4^{4-}$ (Pt-pop),[6] which exhibits electronic absorption bands at 367 and 435 nm, assigned to singlet and triplet $d\sigma^* \rightarrow p\sigma$ transitions, respectively, as well as 514 nm phosphorescence ($\tau \sim 9\ \mu s$ at ambient temperature) from the lowest excited triplet and 407 nm fluorescence from a much shorter-lived (8−40 ps) excited singlet.[7] When irradiated at 367 nm, Pt-pop exhibits very rich chemistry, including electron transfer reactions with various substrates; hydrogen atom abstraction from hydrocarbons, alcohols, stannanes, and silanes; halogen atom abstraction from alkyl and aryl chlorides; duplex DNA cleavage; and catalytic conversion of isopropanol to acetone and hydrogen.[6,8]

In contrast to well-studied Rh, Ir, and Pt systems, there has been little research into Pd dimers that may experience d^8-d^8 interactions, and even fewer investigations of their photophysical properties.[9] Several complexes have been reported with Pd−Pd distances ranging from 2.55 to 3.05 Å,[9] shorter than the sum of the van der Waals radii (3.26 Å),[10] but there has been no agreement on whether a metal−metal bond is present. The limited photophysical investigations have been inconclusive; a weak Pd−Pd bonding interaction in the model compounds $[Pd(CN_2)(PH_3)_2]_2$ (Pd−Pd = 3.107 Å) and $[Pd(CN)_2(\mu\text{-}PH_2CH_2PH_2)]_2$ (Pd−Pd = 3.020 Å) was suggested on the basis of MP2 and time-dependent density functional theory (TDDFT) calculations.[9b,c] Although SCF-Xα-SW calculations on the model compound $[Pd(HNCHNH)_2]_2$ predicted an even *shorter* Pd−Pd distance (2.622 Å), it was concluded that there was *no* bonding interaction.[11]

As part of an investigation into selective oxidation catalysts,[12] we have studied several members of a family of $[(2\text{-arylpyridine})Pd^{II}(O_2CR_3)]_2$ dimers; notably, there has been considerable recent interest in these and related species as precursors to $Pd^{III}-Pd^{III}$ or $Pd^{II}-Pd^{IV}$ dimers that are catalytically active for C−C bond-forming reactions.[13] Here, we present spectroscopic data combined with theoretical analyses, using both DFT and atoms in molecules (AIM) methods, that strongly support the presence of weakly bonding d^8-d^8 interactions in these dimers. We extend our results to a number of other Pd^{II} species with short Pd−Pd distances and demonstrate that the ordering of unoccupied molecular orbitals differs from that found for Rh, Ir, and Pt dimers containing d^8-d^8 interactions, thereby accounting for striking differences in photophysical properties and reactivities.

Results and Discussion

Synthesis and Solid State Structures. The structure of $[(2\text{-phenylpyridine})Pd(\mu\text{-OAc})]_2$ (**1**), which also has been reported elsewhere,[14] does not exhibit the expected planar geometry (of approximate D_{2h} symmetry) but instead resembles an open "clamshell" in which the acetate ligands are perpendicular to the plane containing the Pd atoms and 2-phenylpyridine ligands, with the Pd atoms brought quite close to one another, 2.86216(11) Å.[15] We also synthesized the known compound $[(2\text{-}p\text{-tolylpyridine})Pd(\mu\text{-OAc})]_2$ (**2**) and two closely related species, $[(2\text{-phenylpyridine})Pd(\mu\text{-TFA})]_2$ (**3**) and $[(2\text{-}p\text{-tolylpyridine})Pd(\mu\text{-TFA})]_2$ (**4**), using a modification of a literature procedure.[16] The structures of **1**−**4** are closely related: all four molecules adopt the clamshell geometry (Figure 2 and Table 1), a consequence, we suggest, of both an attractive d^8-d^8 interaction between the two Pd centers and a parallel displaced (slipped) π-stacking interaction between the phenylpyridine rings.[17] In all structures, the distances between

(6) Roundhill, D. M.; Gray, H. B.; Che, C.-M. *Acc. Chem. Res.* **1989**, *22*, 55.
(7) (a) Che, C.-M.; Butler, L. G.; Gray, H. B. *J. Am. Chem. Soc.* **1981**, *103*, 7796. (b) Fordyce, W. A.; Brummer, J. G.; Crosby, G. A. *J. Am. Chem. Soc.* **1981**, *103*, 7061.
(8) Kalsbeck, W. A.; Grover, N.; Thorp, H. H. *Angew. Chem., Int. Ed.* **1991**, *30*, 1517.
(9) (a) Yip, H.-K.; Lai, T.-F.; Che, C.-M. *J. Chem. Soc., Dalton Trans.* **1991**, 1639. (b) Xia, B.-H.; Che, C.-M.; Zhou, Z.-Y. *Chem.—Eur. J.* **2003**, *9*, 3055. (c) Pan, Q.-J.; Zhang, H.-X.; Zhou, X.; Fu, H.-G.; Yu, H.-T. *J. Phys. Chem. A* **2007**, *111*, 287. (d) Clement, S.; Aly, S. M.; Bellows, D.; Fortin, D.; Strohmann, C.; Guyard, L.; Abd-El-Aziz, A. S.; Knorr, M.; Harvey, P. D. *Inorg. Chem.* **2009**, *9*, 4118.
(10) Bondi, A. *J. Phys. Chem.* **1964**, *68*, 441.
(11) Cotton, F. A.; Matusz, M.; Poli, R.; Feng, X. *J. Am. Chem. Soc.* **1988**, *110*, 1144.
(12) Bercaw, J. E.; Day, M. W.; Golisz, S. R.; Hazari, N.; Henling, L. M.; Labinger, J. A.; Schofer, S. J.; Virgil, S. *Organometallics* **2009**, *28*, 5017.
(13) (a) Powers, D. C.; Ritter, T. *Nat. Chem.* **2009**, *1*, 302. (b) Deprez, N. R.; Sanford, M. S. *J. Am. Chem. Soc.* **2009**, *131*, 11234.
(14) (a) Thu, H.-Y.; Yu, W.-Y.; Che, C.-M. *J. Am. Chem. Soc.* **2006**, *128*, 9048. (b) Dinçer, M.; Özdemir, N.; Günay, M. E.; Çetinkaya, B. *Acta Crystallogr. Sect. E: Struct. Rep. Online* **2008**, *E64*, m381.
(15) The two previously reported structures of **1** are polymorphs.[14] In this paper, we report a low temperature structure (100 K) of **1**, which is the same polymorph as reported by Dinçer and co-workers.[14b] For the sake of accurate comparison with other compounds reported here, we use the geometrical parameters from our structure in further discussions.
(16) Aiello, I.; Crispini, A.; Ghedini, M.; La Deda, M.; Barigelletti, F. *Inorg. Chim. Acta* **2000**, *308*, 121.
(17) Janiak, C. *J. Chem. Soc., Dalton Trans.* **2000**, 3885.

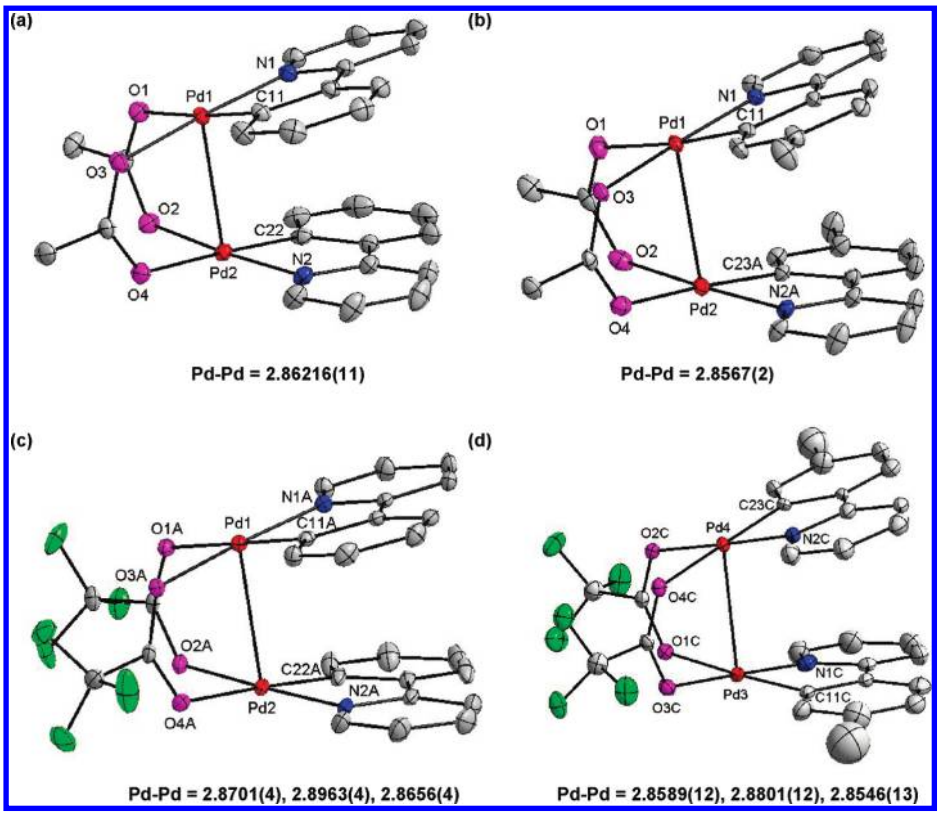

Figure 2. Structures of (a) [(2-phenylpyridine)Pd(μ-OAc)]$_2$ (**1**), (b) [(2-*p*-tolylpyridine)Pd(μ-OAc)]$_2$ (**2**; only major conformation drawn), (c) [(2-phenylpyridine)Pd(μ-TFA)]$_2$ (**3**), and (d) [(2-*p*-tolylpyridine)Pd(μ-TFA)]$_2$ (**4**; only major conformation drawn). All H atoms were omitted for clarity.

Table 1. Selected Bond Distances in **1**−**4**

	1	**2**	**3**[a]	**4**[a]
Pd(1)−C(11)	1.9566(8)	1.956(2)	1.969(3), 1.958(3), 1.960(4)	1.946(5), 1.925(7), 1.897(15)
Pd(1)−N(1)	2.0116(6)	2.0161(17)	2.008(3), 2.009(3), 2.005(3)	1.982(6), 1.974(6), 2.037(13)
Pd(1)−O(3)	2.0473(5)	2.0474(14)	2.093(2), 2.111(3), 2.096(2)	2.062(9), 2.081(7), 2.088(8)
Pd(1)−O(1)	2.1428(6)	2.1378(16)	2.171(2), 2.152(2), 2.184(3)	2.172(8), 2.120(7), 2.132(8)
Pd(1)−Pd(2)	2.86216(11)	2.8567(2)	2.8701(4), 2.8963(4), 2.8656(4)	2.8589(12), 2.8801(12), 2.8546(13)
Pd(2)−C(22)	1.9616(7)	1.937(2)	1.960(4), 1.964(4), 1.976(4)	1.792(9), 1.974(6), 1.894(6)
Pd(2)−N(2)	2.0052(6)	2.0590(16)	2.000(3), 1.964(4), 1.998(4)	2.195(10), 1.999(6), 2.027(6)
Pd(2)−O(2)	2.0520(6)	2.0636(17)	2.077(3), 2.097(3), 2.074(3)	2.088(11), 2.106(8), 2.096(8)
Pd(2)−O(4)	2.1562(5)	2.1407(15)	2.163(2), 2.133(3), 2.156(2)	2.117(10), 2.157(7), 2.145(9)

[a] Three independent conformations.

the ring centroids vary from 3.70 Å to over 4 Å, and the angles between the ring normal of the plane and the centroid vector are between 20° and 40°, consistent with the approximate upper limits for significant interaction.[17] The π stacking between the phenylpyridine rings presumably contributes to the short Pd−Pd distance, but we believe that the d^8−d^8 interaction plays the main role in determining the overall geometry because in principle the molecule could π-stack just as effectively if it were planar. The structures of the TFA bridged species **3** and **4** both contain three independent molecules, with similar bond distances and angles in the asymmetric unit, while there is disorder associated with the methyl groups of the 2-*p*-tolylpyridine ligands in **2** and **4**. The Pd−Pd distance decreases by approximately 0.01 Å when moving from phenylpyridine to the more electron-donating 2-*p*-tolylpyridine, while moving from OAc to the less electron-donating TFA increases the distance by 0.01 Å.

An interesting feature of the molecules is the relative orientation of the 2-arylpyridine rings, which may either be "cis", with both pyridine rings opposite one other (approximate C_s symmetry), or "trans", with each pyridine ring opposite a benzene ring (approximate C_2 symmetry). In **1** and **3**, it is impossible to distinguish between all-cis or a 50%−50% mixture of cis and trans (for which crystallographic averaging would give the observed structure). However, the structure of **2**, though disordered, shows a preference for the trans orientation, with only approximately 15% cis. The structure of **4** is even more highly disordered, but both orientations can be observed, again with a preference for trans.

In order to assess the presence of Pd−Pd bonding interactions by photophysics, we also examined control samples. The structures of the previously reported[18] complexes [(2-phenylpyridine)Pd(μ-Cl)]$_2$ (**5**) and [(2-phenylpyridine)-Pd(en)][Cl] (**6**, en = ethylenediamine) indicate the absence of any Pd−Pd interaction. Complex **5** has a nearly flat structure, in contrast to those of **1**−**4**, with the bridging chlorides almost coplanar with the 2-phenylpyridine ligands

(18) Craig, C. A.; Watts, R. J. *Inorg. Chem.* **1989**, *28*, 309.

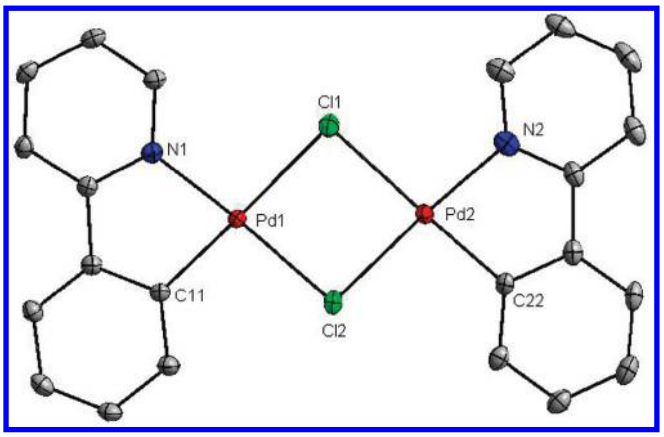

Figure 3. Structure of [(2-phenylpyridine)Pd(μ-Cl)]$_2$ (**5**). All H atoms were omitted for clarity. Selected bond distances (Å) of **5**: Pd(1)−C(11), 1.9865(10); Pd(1)−N(1), 2.0134(9); Pd(1)−Cl(2), 2.3633(3); Pd(1)−Cl(1), 2.4233(3); Pd(2)−C(22), 1.9869(10); Pd(2)−N(2), 2.0146(10); Pd(2)−Cl(2), 2.3725(3); Pd(2)−Cl(1), 2.4271(3).

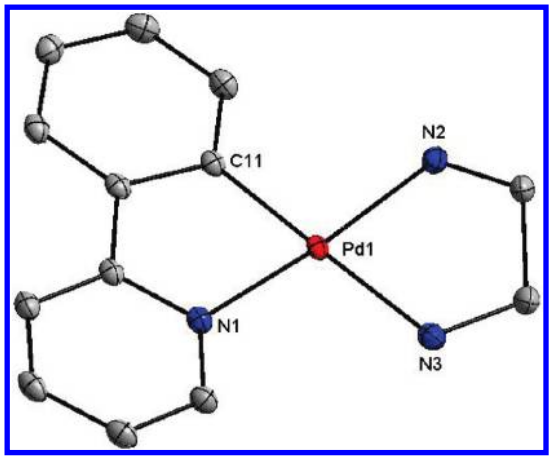

Figure 4. Structure of [(2-phenylpyridine)Pd(en)][Cl] (**6**). All H atoms and the Cl$^-$ anion were omitted for clarity. Selected bond distances (Å) of **6**: Pd(1)−C(11), 1.9849(12); Pd(1)−N(1), 2.0195(9); Pd(1)−N(2), 2.0652(10); Pd(1)−N(3), 2.1443(11).

(Figure 3). The dimeric units are stacked, but the closest Pd−Pd contact is 3.691 Å, which is significantly larger than the sum of the van der Waals radii of two Pd atoms. Complex **6** exhibits normal square planar coordination geometry (Figure 4); the closest intermolecular Pd−Pd distance is greater than 5 Å.

Electrochemistry. Cyclic voltammograms of **1**−**4** in CH_2Cl_2 are shown in Figure 5; differential pulse voltammetry (Figure 6) was used to further resolve the electrochemical features (Table 2). Compounds **1** and **2** show one reversible peak (390 and 350 mV, respectively) assigned to $Pd^{III}-Pd^{II}/Pd^{II}-Pd^{II}$ and one irreversible peak (710 and 740 mV) assigned as the $Pd^{III}-Pd^{III}/Pd^{II}-Pd^{III}$ couple. The decreased area under the second peak is attributable to disproportionation of the $Pd^{II}-Pd^{III}$ mixed-valence state:

$$2Pd^{II}-Pd^{III} \rightarrow Pd^{II}-Pd^{II} + Pd^{III}-Pd^{III}$$

Such processes also occur in electrochemically generated $Rh(d^8)-Rh(d^7)$ systems.[19] Irreversible oxidation of the ligand occurs at anodic potentials greater than 1 V (Figure S1, Supporting Information). The $Pd^{III}-Pd^{II}/Pd^{II}-Pd^{II}$ couple is shifted anodically by 300 mV in **3** and **4**, and a second Pd−Pd redox event is not observed before the onset of ligand oxidation. We believe that the shift to higher potentials seen as the bridging ligand is changed from acetate to trifluoroacetate reflects increased withdrawal of electron density from Pd_2, stabilizing the highest occupied molecular orbital (HOMO) and rendering oxidation more difficult. The potentials of $Pd^{II}-Pd^{III}/Pd^{II}-Pd^{II}$ as well as $Pd^{III}-Pd^{III}/Pd^{II}-Pd^{III}$ couples in **1** and **2** are comparable with those reported recently for a binuclear palladium benzoquinoline acetate complex.[13a]

A cyclic voltammogram (CV) for **5** could not be obtained in CH_2Cl_2 owing to solubility problems; however, measurements made in acetonitrile reveal a single irreversible oxidation near 820 mV, assigned to $Pd^{II}-Pd^{III}/Pd^{II}-Pd^{II}$ (Figure S2, Supporting Information). The CVs for **1**−**4** in acetonitrile are surprisingly different from those reported in CH_2Cl_2 (Table 3). The potential associated with the first oxidation depends strongly on the identity of the bridging ligand, ranging from 380 mV

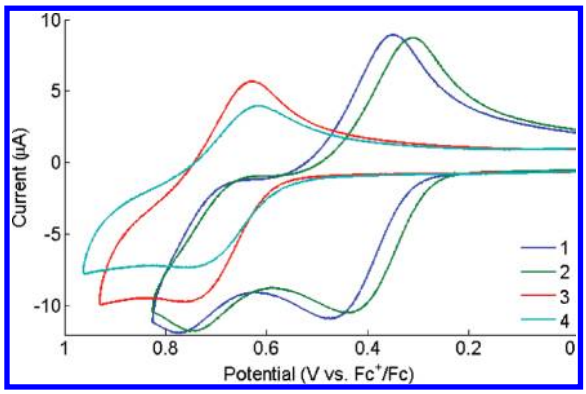

Figure 5. Cyclic voltammograms of **1**−**4** in CH_2Cl_2 solution.

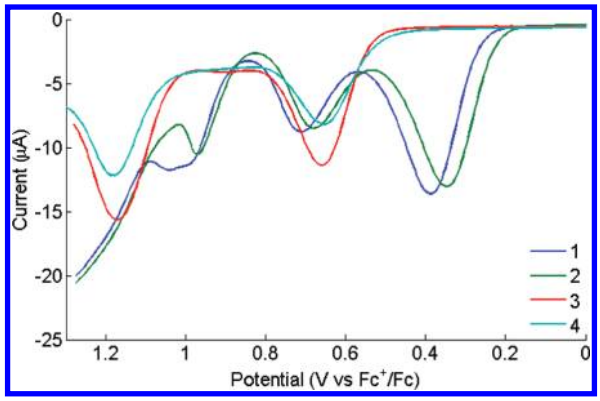

Figure 6. Differential pulse voltammograms of compounds **1**−**4** in CH_2Cl_2 solution.

Table 2. Reduction Potentials for Compounds **1**−**4** (mV vs Fc^+/Fc) from DPV Experiments in CH_2Cl_2

compound	$Pd^{II}-Pd^{III}/Pd^{II}-Pd^{II}$	$Pd^{III}Pd^{III}/Pd^{II}-Pd^{III}$
1	390	710
2	350	680
3	660	not observed
4	660	not observed

(19) Mann, K. R.; Hill, M. G. *Catal. Lett.* **1991**, *11*, 341.

Table 3. Reduction Potentials for Compounds **1**−**5** (mV vs Fc^+/Fc) from DPV Experiments in CH_3CN

compound	$Pd^{II}-Pd^{III}/Pd^{II}-Pd^{II}$	$Pd^{III}-Pd^{III}/Pd^{II}-Pd^{III}$
1	430	1400
2	380	1350
3	1160	1400
4	1180	1370
5	820	1340

(vs Fc^+/Fc) for acetate-bridged **2** to 1180 mV for TFA-bridged **4**, a difference that is much larger than we would have expected. Of greater interest is that the experiments in acetonitrile show clearly that **1** and **2** are more easily oxidized than **5**, which is consistent with our electronic structural model: the HOMO is Pd−Pd antibonding in **1** and **2**; it is nonbonding in **5**. DFT calculations (see below and the Supporting Information for details) are consistent with the experimentally determined reduction potentials. Unfortunately, reliable electrochemical data were not obtained for **6**, owing to its low solubility in both acetonitrile and CH_2Cl_2.

Photophysics. UV−vis absorption spectra of **1**−**6** (Figure 7) follow Beer's Law, indicating that aggregration does not occur at concentrations below 200 μM. Intense absorption bands are observed at wavelengths shorter than 350 nm, with molar absorptivities greater than 5000 M^{-1} cm^{-1} (Table 4). Compounds **1** and **2** exhibit weaker absorptions with maxima at 420 nm ($\varepsilon = 2000$ M^{-1} cm^{-1}), whereas absorptions of **3** and **4** in the visible region are broad and featureless. The absorption profiles of **5** and **6** are very similar to those of **1**−**4** in the UV region, but not at wavelengths greater than 380 nm. The higher-energy bands are attributable to [$\pi-\pi^*$] intraligand (IL) transitions, and the visible absorption peaks in the spectra of **1** and **2** are assigned to [$d\sigma^*(Pd_2)-\pi^*$(ppy)] metal−metal to ligand charge transfer (MMLCT). MMLCT transitions of **3** and **4** are observed as absorptions at higher energy that tail into the visible region. The blue shift is attributable to electron withdrawal from Pd_2 to the bridging TFA ligands, which stabilizes the $d\sigma^*(Pd_2)$ HOMO. The electronic spectrum of **5**, where the Pd−Pd distance is greater than 3.6 Å, is very similar to that of monometallic **6**.

Luminescence was not detected from any of the compounds **1**−**6** at room temperature; however, all were found to luminesce upon cooling to cryogenic temperatures. Excitation (355 nm) of samples in 2-methyltetrahydrofuran (2-MTHF) glasses at 77 K reveals richly structured emission features in the 450−600 nm region. Notably, there is a sharp peak at 461 nm in the emission spectrum of **1** (Figure 8), and the spectra of **3**, **5**, and **6** are similar. The sharp feature is red-shifted by 5 nm in **2** and **4** (Table 4). The 450−600 nm emission system in each case likely is attributable to an electronic transition that involves a mixture of ligand-centered [$\pi-\pi^*$] and metal-to-ligand charge transfer (MLCT) components. Vibronic peaks spaced by 1200 cm^{-1} indicate that this transition is coupled to aromatic ring-breathing modes. Additional structure on these features with approximately 400 cm^{-1} spacings suggests that there also is excitation of ground state Pd−L stretching vibrations. Importantly, the **1**−**4** 450−600 nm emission profiles are similar to those of monomeric metal−phenylpyridine complexes.[20]

(20) Ivanov, M. A.; Puzyk, M. V. *Opt. Spectrosc.* **2001**, *91*, 927.

Emission spectra of complexes **1**−**4** (which have short Pd−Pd distances) also exhibit a broad system that peaks at 740 nm. This low-energy band (without any hint of vibronic structure at 77 K) is not observed in the spectra of monomeric phenylpyridine complexes (e.g., **6**) or the phenylpyridine chloride dimer **5**. We assign this feature to a MMLCT transition, in accord with our calculations of the relative energies of $d\sigma^*(Pd_2)$ HOMO and ligand π^* lowest unoccupied molecular orbital (LUMO) levels (see below). Upon changing the excitation wavelength to 420 nm, the 460 nm emission quantum yields of **1**−**4** decrease markedly, but the 740 nm emission intensity is largely unaffected. On varying the excitation wavelength from 300 to 420 nm and monitoring the luminescence of **1** and **2** at 460 nm, we found that the absorption and excitation spectra are similar between 300 and 380 nm, but not from 380 to 420 nm, a region in which the emission intensity is extremely weak. When a similar experiment was conducted while monitoring emission at 790 nm, the excitation spectrum followed absorbance through the visible region (Figure 9). We therefore suggest that there are two competitive pathways for deactivation of the higher-energy IL ($\pi-\pi^*$) excited state: one is direct radiative decay to the ground state, and the other is relatively slow internal conversion to the MMLCT excited state.

Measurements of radiative decay kinetics have shed light on the nature of the excited state dynamics. With excitation at 355 nm, decays from **1**−**4** monitored at both 460 and 720 nm are biexponential, with lifetimes in microsecond ranges. In contrast, emission decay from electronic excitation of the chloro-bridged species **5** is monoexponential, with a lifetime consistent with those determined at 77 K for other M(ppy) complexes.[20] All emission spectra recorded at 460 nm also exhibited a short-lived fluorescence component.[21] We tentatively suggest that the biexponential kinetics associated with **1**−**4** emissions are attributable to electronically excited stereoisomers (*cis*- or *trans*-N−Pd−Pd−N geometry) in the 77 K glasses.[22]

Density Functional Theory Analysis of Bonding in Compounds 1−**5.** DFT studies were performed on **1** (with no symmetry constraints, which also serves as a model for **2**), **3** (with no symmetry constraints, which also serves as a model for **4**), and **5** (modeled using C_{2h} symmetry). In general, there was good agreement between experimental and calculated structures, which suggests that our model is able to reproduce key structural parameters.[23] The

(21) Kim, C. D.; Pillet, S.; Wu, G.; Fullagar, W. K.; Coppens, P. *Acta Crystallogr., Sect. A: Found. Crystallogr.* **2002**, *58*, 133.

(22) Advances in separation techniques have opened the way for more rigorous investigations of the excited state properties of stereoisomers of organic and inorganic compounds, see: (a) Keene, F. R. *Coord. Chem. Rev.* **1997**, *166*, 121. Typically, optical isomers have shown minimal differences in excited state behavior, see: (b) Rutherford, T. J.; Van Gijte, O.; Kirsch-De Mesmaeker, A.; Keene, F. R. *Inorg. Chem.* **1997**, *36*, 4465 or (c) Browne, W. R.; O'Connor, C. M.; Villani, C.; Vos, J. G. *Inorg. Chem.* **2001**, *40*, 5461. However, differences are more pronounced for geometric isomers, where excited state lifetimes in some cases vary by more than an order of magnitude, see: (d) Spalletti, A.; Bartocci, G.; Galiazzo, G.; Macchioni, A.; Mazzucato, U. *J. Phys. Chem. A* **1999**, *103*, 8994. (e) Treadway, J. A.; Chen, P.; Rutherford, T. J.; Keene, F. R.; Meyer, T. J. *J. Phys. Chem. A* **1997**, *101*, 6824 or (f) Booth, E. C.; Bachilo, S. M.; Kanai, M.; Dennis, T. J. S.; Weisman, R. B. *J. Phys. Chem. C* **2007**, *111*, 17720.

(23) See the Supporting Information for more details.

Table 4. Absorption and Emission Data

compound	absorption, λ_{max}/nm (ε_{max}/M^{-1} cm^{-1})	emission,[a] λ_{em}/nm (τ_o/μs)
1	305 (10300), 315 (8100), 350 (5900), 410 (1800)	461 (180 (70%), 70 (30%)), 740 (150 (50%), 60 (50%))
2	309 (10000), 322 (8500), 347 (7200), 373 (5000), 410 (2300)	466 (240 (70%), 110 (30%)), 740 (65 (40%), 12 (60%))
3	307 (11800), 317 (11400), 343 (7300), 362 (5400), 400 (2300)	461 (290 (70%), 80 (30%)), 740 (50 (20%), 10 (80%))
4	313 (11700), 322 (12200), 347 (8800), 370 (4000), 400 (1900)	466 (250 (80%), 50 (20%)), 740 (60 (30%), 10 (70%))
5	307 (13800), 317 (14700), 360 (4500)	461 (320)
6	305(4100), 317 (4400), 338 (3300)	461 (350)

[a] Measurements were made on samples in 2-MTHF glasses at 77 K (λ_{ex} = 355 nm).

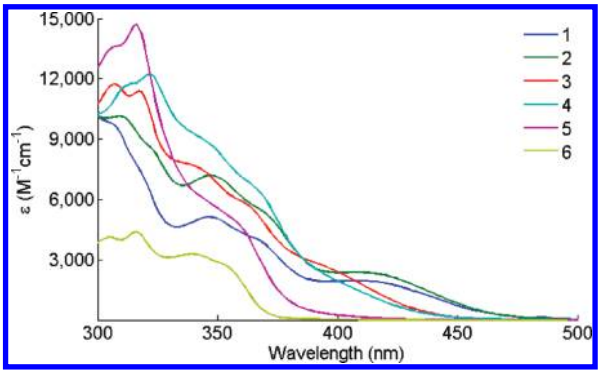

Figure 7. Electronic absorption spectra of **1**−**6** in 2-MTHF solutions.

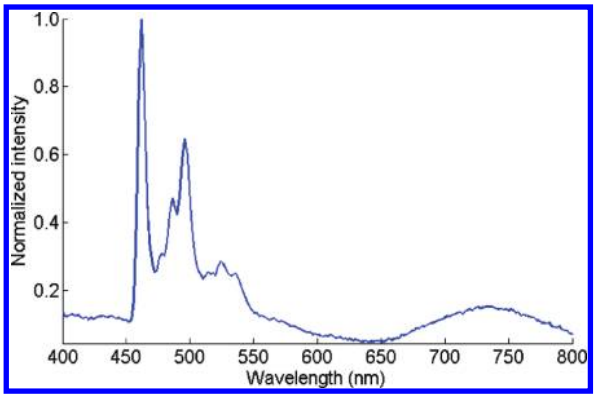

Figure 8. Emission spectrum of **1** in a 2-MTHF glass at 77 K (λ_{ex}=355 nm).

calculations on **1** and **3** show that the HOMO is a d_{z^2} σ* Pd−Pd antibonding orbital, while the LUMO and close-lying empty orbitals are located on the 2-phenylpyridine rings and possess mainly ligand character. The Pd−Pd σ-bonding character (a mixture of both d_{z^2} and d_{xy}) is spread over two MOs (91 and 93) and mixes with both the bridging acetate and 2-phenylpyridine ligands. As expected, there are a number of occupied nonbonding metal orbitals and ligand-based orbitals between the HOMO and the Pd−Pd bonding orbitals. Selected molecular orbitals of **1**, with the percentage contributions from different Pd atomic orbitals, are shown in Figure 10.

A fragment analysis was performed in which **1** was broken into Pd_2, $(phenylpyridine)_2$, and $(OAc)_2$ units; the resulting molecular orbital diagram is shown in Figure 11. The analysis confirms that the LUMO and slightly higher-energy orbitals are based on the 2-phenylpyridine ligands. Importantly, it shows that, although the HOMO is predominantly formed from the Pd d_{z^2} orbitals, there also are small contributions from the 5s and $5p_z$ orbitals

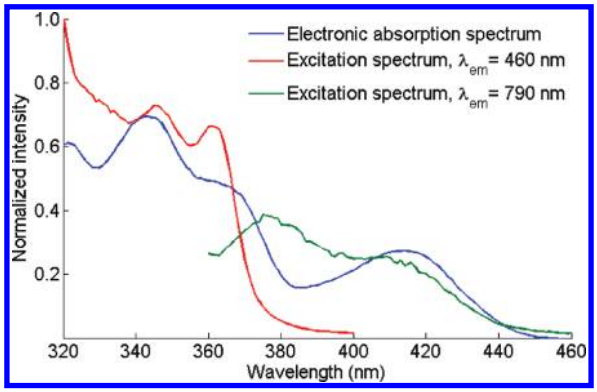

Figure 9. Absorption and excitation spectra of **2** in 2-MTHF at 77 K.

due to symmetry-allowed mixing (the HOMO in Figure 10 is a linear combination of the 5s and $5p_z$ orbitals). Similar mixing occurs in the orbitals with Pd−Pd bonding character (91 and 93), although the contribution from the 5s and $5p_z$ orbitals is smaller due to the greater disparity in orbital energies. The overall effect of this mixing is to increase overlap in the bonding interaction while decreasing overlap in the antibonding interaction; a Pd−Pd bond order of 0.11 was calculated for **1**.[24] This is consistent with a weak bonding interaction and suggests the presence of d_{z^2}, p_z, and s orbital mixing in **1**−**4**, similar to that described earlier for Pt-pop. The AIM approach,[25] which uses topological analysis of the electron distribution to characterize bonding interactions, confirms the presence of metal−metal bonding interactions in **1** and **3**. In both cases (3, −1), bond critical points (indicative of the presence of a bonding interaction)[26] centered between the two Pd atoms were found. The ellipticity values were 0.004 and 0.003, respectively, indicating a σ bonding interaction.

Frequency calculations on **1** and **3** gave Pd−Pd symmetric and asymmetric stretches around 120−130 cm^{-1}, both heavily coupled to other vibrations such as ring-breathing modes. We were unable to obtain direct experimental evidence for a Pd−Pd bonding interaction from polarized single-crystal Raman spectroscopy or low-temperature UV−vis spectroscopy, presumably because of this coupling to other bonding modes and the absence of a well-defined uncoupled d_{z^2} σ* to pσ transition. In

(24) Cloke, F. G. N.; Green, J. C.; Jardine, C. N.; Kuchta, M. C. *Organometallics* **1999**, *18*, 1087.

(25) Bader, R. F. W. *Atoms in Molecules: A Quantum Theory*; Oxford University Press: New York, 1994.

(26) (a) Bader, R. F. W. *Chem. Rev.* **1991**, *91*, 893. (b) A (3,−1) critical point is a point at which the electron density is a minimum in the direction of the two bonded atoms and a maximum in the two orthogonal directions. It is taken as indicative of a covalent bond.

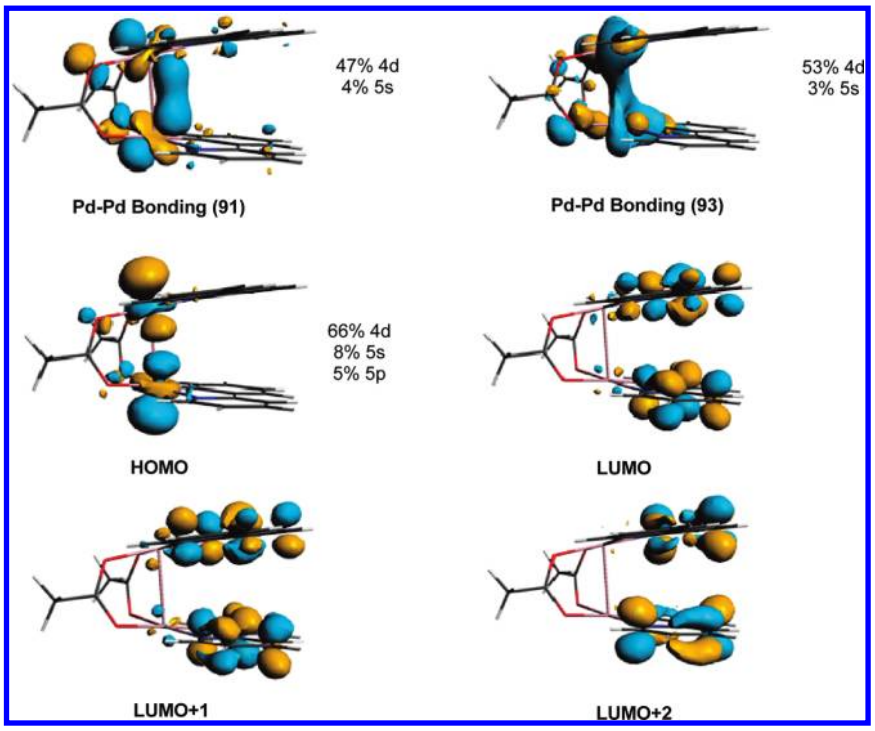

Figure 10. Selected molecular orbitals of **1**, with percentage contribution from different Pd atomic orbitals (balance from ligand-based orbitals).

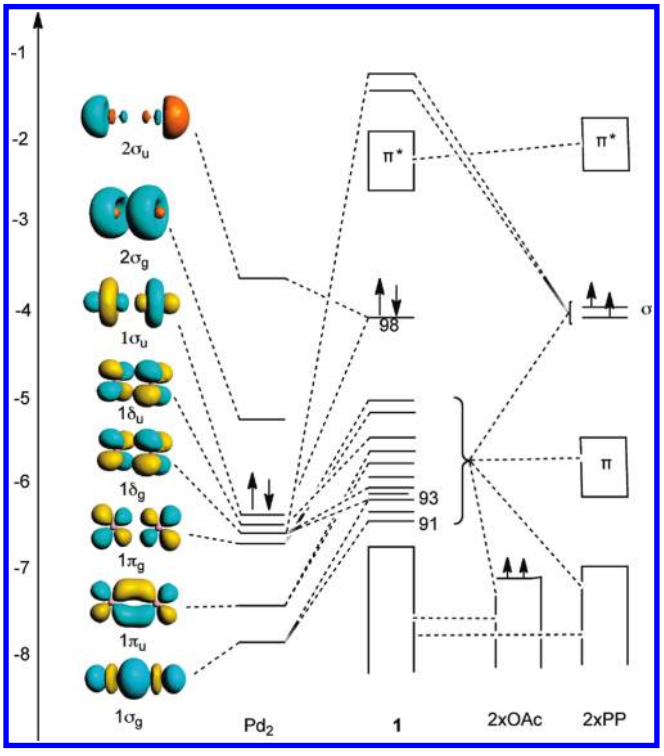

Figure 11. Molecular orbital diagram for **1**.

contrast, a highly polarized Pt−Pt stretch has been observed at 118 cm^{-1} in the Raman spectrum of Pt-pop.[27]

Calculations on planar [(2-phenylpyridine)Pd(μ-Cl)]$_2$ (**5**) showed no overlap between the valence d_{z^2} orbitals on the two Pd atoms and hence no Pd−Pd bonding interaction. Instead, there are two essentially degenerate nonbonding linear combinations of the d_{z^2} orbitals, which are of a similar energy to the nonbonding linear combinations of other Pd d orbitals. As in **1** and **3**, the LUMO and close-lying empty orbitals of **5** are centered on the 2-phenylpyridine ligands. The HOMO−LUMO gap in **5** (2.40 eV) is much larger than in **1** (1.53 eV) or **3** (1.60 eV) because the HOMO in **5** is nonbonding, whereas in **1** and **3** it is an antibonding d_{z^2} Pd−Pd interaction, raised in energy relative to the π^* system of the 2-phenylpyridine ligands. The larger HOMO−LUMO gap in **5** compared with **1** and **3** is consistent with the UV−visible spectroscopy, which showed bands at lower energy in **1**−**4** than in **5**, providing further evidence supporting our assignment of the bands at approximately 420 nm in **1** and **2** as MMLCT transitions (excitation from the Pd−Pd antibonding orbital into the 2-phenylpyridine π^* system); these bands are shifted to around 375 nm in **3** and **4** and absent in **5**. Furthermore, imposition of a C_2 symmetry constraint allowed optimization of structure **1** in the excited configuration, with one electron promoted from the HOMO to the LUMO; the resulting Pd−Pd distance is 2.6 Å, consistent with an increase in the Pd−Pd bond order and a large geometry change between the ground (calculated Pd−Pd distance = 2.8 Å) and excited states, which may explain the large Stokes shift observed in the emission from **1** on excitation at 420 nm.

DFT-Based Comparison of Bonding Interactions in Pd−Pd d^8 Dimers with Those in Rh−Rh, Pt−Pt, and Ir−Ir d^8 Dimers. The results of the spectroscopic and computational studies on compounds **1**−**4** suggest that the Pd−Pd bonding interaction is different from the d^8−d^8 interactions in Rh, Pt, and Ir dimers. In the latter systems, the LUMO is a metal−metal bonding orbital with s and p_z character, whereas in **1**−**4** the LUMO and other close-lying unoccupied orbitals are ligand-based. Indeed, it

(27) Che, C.-M.; Butler, L. G.; Gray, H. B.; Crooks, R. M.; Woodruff, W. H. *J. Am. Chem. Soc.* **1983**, *105*, 5492.

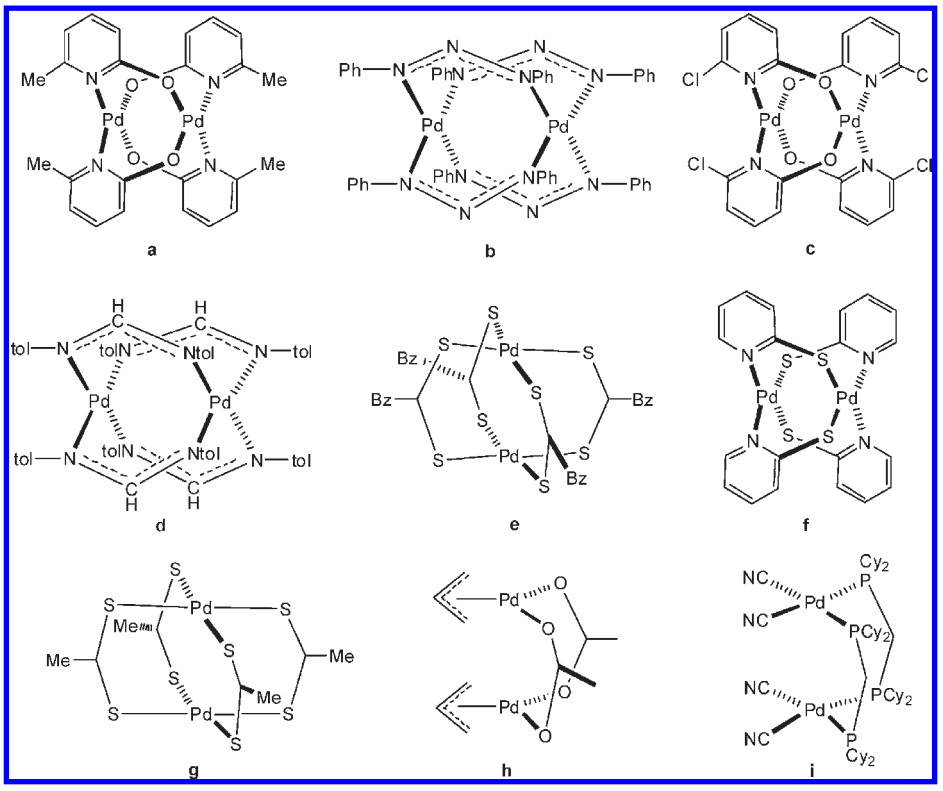

Figure 12. Complexes with short Pd−Pd interactions selected for DFT calculations.[9]

appears that the energy of the metal−metal bonding p_z orbital in **1**−**4** is much higher than the LUMO, which may explain why the unique photophysical properties arising from a d_{z^2} σ^* to pσ transition in Pt-pop and other d^8−d^8 dimers are not observed in the Pd dimers. To explore whether the absence of a low-energy d_{z^2} σ^* to pσ transition is general to Pd complexes with short Pd−Pd interactions or is unique to **1**−**4**, we performed calculations on the complexes cited earlier,[9] shown as **a**−**h** in Figure 12, as well as on Pt-pop (Pt−Pt = 2.925(1)),[21,28] [(cod)Ir(μ-pyr)]$_2$ (**j**, cod = 1,5-cyclooctadiene, pyr = pyrazole, Ir−Ir = 3.216(5) Å),[29] and $[Rh(CNMe)_4]_2^{2+}$ (**k**) as a model for $[Rh(CNPh)_4]_2^{2+}$ (Rh−Rh = 3.193(0)Å)[30] (Figure 13).

For all of the Pd complexes, the calculated HOMO is an antibonding combination of the d_{z^2} orbitals, with a small contribution from the 5s and 5p_z orbitals, similar to that described earlier for **1**.[23] The complementary Pd−Pd σ-bonding orbital is at lower energy and also has some contribution from the 5s and 5p_z orbitals. For all of the compounds, fragment analysis reveals a favorable bonding interaction, with the bond order varying from 0.1 to 0.56 (this is a measure of positive orbital overlap rather than bond strength). Additional support for the presence of a Pd−Pd bonding interaction was obtained from AIM analysis: there is an excellent correlation between the Pd distance and both the charge density and the Laplacian at the bond critical points (Figure 14), suggesting that the Pd−Pd bonding interaction is related to the separation between the Pd atoms.

The calculations also showed that the LUMO and close-lying empty orbitals in the Pd complexes are not based on a bonding linear combination of the s and p_z orbitals. Instead, the LUMO consists of either ligand-based orbitals or, when there are no low-lying unoccupied ligand orbitals, an antibonding combination of Pd $d_{x^2-y^2}$ and ligand orbitals.[23] In contrast, calculations on Pt-pop and [(cod)Ir(μ-pyr)]$_2$ (**j**) showed that the LUMO is a metal-based bonding orbital, which contains both s and p_z character.[31] These results suggest that the larger gap between the $(n+1)$ valence s and p orbitals and the valence d orbitals for Pd compared with Ir or Pt is crucial in determining the relative energy of the unoccupied orbitals in d^8−d^8 dimers. Even in $[Rh(CNMe)_4]_2^{2+}$ (**k**), the LUMO contains some s and p character mixed with a large ligand contribution, suggesting that the gap between Pd 5s and 5p orbitals and the 4d orbitals is large even compared to other elements in the same row. These trends are reflected in the atomic spectra of Rh, Pd, Ir, and Pt (Table 5); the lowest Pd d to p transition is nearly 10 000 cm^{-1} higher than a corresponding transition in the other metals.[32] The ground state atomic configuration of Pd ($4d^{10}$) is also consistent with a larger gap between d and s and p orbitals relative to Rh ($4d^8$, $5s^1$), Ir ($5d^7$, $6s^2$), and Pt ($5d^9$, $6s^1$).

Since many of the interesting photophysical and reactivity properties of Pt-pop, Rh−Rh, and Ir−Ir d^8−d^8

(28) (a) Filomena Dos Remedios Pinto, M. A.; Sadler, P. J.; Neidle, S.; Sanderson, M. R.; Subbiah, A.; Kuroda, R. *J. Chem. Soc., Chem. Commun.* **1980**, 13. (b) Marsh, R. E.; Herbstein, F. H. *Acta Crystallogr., Sect. B: Struct. Sci.* **1983**, *39*, 280.

(29) Coleman, A. W.; Eadie, D. T.; Stobart, S. R.; Zaworotko, M. J.; Atwood, J. L. *J. Am. Chem. Soc.* **1982**, *104*, 922.

(30) Mann, K. R.; Lewis, N. S.; Williams, R. M.; Gray, H. B.; Gordon, J. G., II. *Inorg. Chem.* **1978**, *17*, 828.

(31) (a) Novozhilova, I. V.; Volkov, A. V.; Coppens, P. *J. Am. Chem. Soc.* **2003**, *125*, 1079. (b) Pan, Q.-J.; Fu, H.-G.; Yu, H.-T.; Zhang, H.-X. *Inorg. Chem.* **2006**, *45*, 8729.

(32) Moore, C. E *Atomic Energy Levels, Vol. III* (*Molybdenum through Lanthanum and Hafnium through Actinium*), Circular of the National Bureau of Standards 467, U.S. Government Printing Office, Washington, DC, 1958.

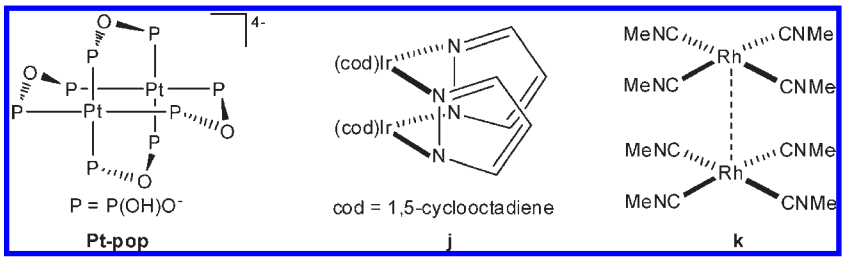

Figure 13. Complexes with d^8-d^8 bonding interactions selected for DFT calculations.

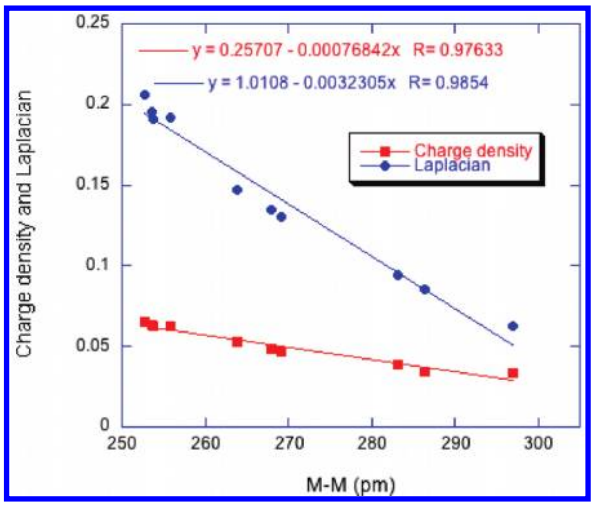

Figure 14. Plot of charge density and Laplacian against the M−M distance in compounds **1** and **a**−**h**.

Table 5. Energy of the nd → (*n* + 1)p Transition As Calculated from Atomic Spectra[32]

metal	nd → (n+1)p/cm^{-1}	transition
Rh	23766	$4d^9$ (^{2}D) → $4d^8$ (^{3}F) 5p (^{4}D°)
Pd	34068	$4d^{10}$ (^{1}S) → $4d^9$ ($^2D_{2\ 1/2}$) 5p (^{3}P)
Ir	23473	$5d^8$ 6s (^{4}F) → $5d^7$ 6s (^{5}F) 6p (^{6}D°)
Pt	26480	$5d^{10}$ (^{1}S) → $5d^9$ ($^2D_{2\ 1/2}$) $6p_{0\ 1/2}$

Table 6. Relative Contribution of the d Orbitals and (*n* + 1) Valence s and p Orbitals to the Metal−Metal Bonding and Antibonding Orbitals in **1**, Pt-pop, $[Rh(CNMe)_4]_2^{2+}$ (**k**), and $[(cod)Ir(\mu\text{-pyr})]_2$ (**j**)[a]

	M−M antibonding	M−M bonding	M−M bonding
1	66% 4d	47% 4d	53% 4d
	8% 5s	4% 5s	3% 5s
	5% 5p		
$[Rh(CNMe)_4]_2^{2+}$ (**k**)	48% 4d	79% 4d	70% 4d
	29% 5s	6% 5s	2% 5s
	2% 5p		
Pt-pop	33% 5d	56% 5d	52% 5d
	50% 6s	23% 6s	7% 6s
	3% 6p	1% 6p	
$[(cod)Ir(\mu\text{-pyr})]_2$ (**j**)	69% 5d[b]	26% 5d	67% 5d[b]
	10% 6s	20% 6s	7% 6s
	1% 6p	1% 6p	

[a] Where numbers do not add up to 100%, the remainder of the orbital is centered on the ligand. [b] The relative d contribution to these orbitals is raised by mixing with a number of d orbitals other than the d_{z^2}.

dimers appear to result from the special nature of the LUMO, we suggest that Pd complexes that display similar behavior may not be attainable, and that the M−M bonding interaction is weaker for Pd because the larger energy difference between the (*n* + 1) valence s and p orbitals and the valence d orbitals disfavors orbital mixing. This view is supported by the relative contributions of the (*n* + 1) valence s and p orbitals to the σ^* HOMO and corresponding metal−metal σ-bonding orbital for **1** compared to Pt-pop, $[(cod)Ir(\mu\text{-pyr})]_2$ (**j**), and $[Rh(CNMe)_4]_2^{2+}$ (**k**) (Table 6). At present, there is no direct experimental data on metal−metal bond strengths that would validate this proposal.

Conclusions

Crystal structure analyses combined with photophysical, electrochemical, and computational investigations have firmly established that there are attractive d^8-d^8 interactions in Pd^{II} dimers of the type $[(2\text{-phenylpyridine})Pd(\mu\text{-X})]_2$ and $[(2\text{-}p\text{-tolylpyridine})Pd(\mu\text{-X})]_2$ (X = OAc or TFA). The Pd−Pd HOMO is a weakly metal−metal antibonding d_{z^2} σ^* orbital, and the LUMO is either a low-lying ligand orbital or a $d_{x^2-y^2}$ antibonding orbital. The M−M interaction in Pd d^8-d^8 dimers is weaker than in Rh, Ir, and Pt systems. The Pd−Pd LUMO also differs from those of d^8-d^8 complexes of Rh, Ir, and Pt, owing to the unusually large energy gap between Pd $4d_{z^2}$ and 5s/5p orbitals. Since the increase in Pd−Pd bond order upon HOMO−LUMO excitation is only one-half that of other metal d^8-d^8 complexes, it is not likely that electronically excited Pd^{II} dimers will be able to abstract hydrogen or halogen atoms from substrates as efficiently as Pt^{II} analogues.

Experimental Section

General. All manipulations were performed in the air, unless otherwise stated. $Pd(OAc)_2$, $Pd(TFA)_2$, 2-phenylpyridine (all purchased from Sigma-Aldrich), and 2-*p*-tolyl-pyridine (purchased from TCI-America) were reagent-grade commercial samples used without further purification. Dichloromethane-d_2 and chloroform-d_1 were purchased from Cambridge Isotope Laboratories and used as received. [(2-Phenylpyridine)Pd(OAc)]$_2$ (**1**), [(2-*p*-tolylpyridine)Pd(OAc)]$_2$ (**2**), [(2-phenylpyridine)Pd(μ-Cl)]$_2$ (**5**), and [(2-phenylpyridine)Pd(en)][Cl] (**6**) were prepared using literature procedures.[16,18,33] ^{1}H and ^{13}C NMR spectra were recorded at 298 K using a Varian Mercury 300 MHz spectrometer equipped with the VNMRJ software program, version 2.2d. ^{1}H and ^{13}C NMR spectra were referenced to the residual proton or carbon chemical shifts of the deuterated solvent. The data are reported by chemical shift (ppm) from tetramethylsilane, multiplicity (s, singlet; d, doublet; t, triplet; m, multiplet; dd, double doublet; dt, double triplet), coupling constants (Hz), and integration. Mass spectra were acquired on a Finnigan LCQ ion trap or Agilent 5973 Network mass selective detector and were obtained by peak matching. UV-vis absorbance spectra were recorded on an Agilent 8453 UV-vis Spectrometer using a pure sample of the solvent as the background. X-ray crystallographic data were collected on a Bruker

(33) Gutierrez, M. A.; Newkome, G. R.; Selbin, J. *J. Organomet. Chem.* **1980**, *202*, 341.

KAPPA APEX II instrument, with the crystals mounted on a glass fiber with Paratone-N oil. Structures were determined using direct methods as implemented in the Bruker AXS software package.

Electrochemistry. Cyclic voltammetry and differential pulse voltammetry were carried out using a 660 Electrochemical Workstation (CH-Instrument, Austin, TX). Measurements were performed at room temperature in CH_2Cl_2 or acetonitrile solutions with 0.1 M $TBAPF_6$ as the supporting electrolyte. The sample concentration was kept at approximately 1 mM. A scan rate of 0.1 V/s was used for all cyclic voltammetry measurements. Experiments were conducted using a glassy carbon working electrode, a saturated Ag/AgCl reference electrode, and a platinum wire counterelectrode. Ferrocenium/ferrocene (Fc^+/Fc) was used as an internal reference.

Steady State and Time-Resolved Luminescence. Low-temperature measurements were conducted on samples in 2-methyltetrahydrofuran glasses. Samples were placed in quartz electron paramagnetic resonance tubes and rigorously degassed with five freeze−pump−thaw cycles. For both time-resolved and steady-state measurements at 77 K, samples were submerged in liquid nitrogen within a homemade quartz optical dewar. Steady state emission spectra were recorded on a Jobin Yvon Spex Fluorolog-3-11. Sample excitation was achieved via a xenon arc lamp with a single monochromator providing wavelength selection. Right angle light emission was sorted using a single monochromator and fed into a Hammamatsu R928P photomultiplier tube with photon counting. Short and long pass filters were used where appropriate. Spectra were recorded on Datamax software. Time-resolved measurements were carried out using 10 ns pulses at 355 nm from Spectra-Physics Quanta-Ray Q-switched Nd:YAG laser operating at 10 Hz. Luminescence decays were detected through an Instruments SA (ISA Edison, NJ) model DH10 (1200 grooves/mm) double monochromator and Hamamatsu R928 PMT with a five-stage socket made by Products for Research (model R928/17149.00301.0040, Bridgewater, NJ). Signals were amplified with a Phillips Scientific 100 MHz bipolar amplifier (100×) and recorded on a Tektronix model TDS-620A digitizing oscilloscope.

Computational Details. Quantum chemical calculations were performed using density functional methods of the Amsterdam Density Functional (Version ADF2007.01) package.[34] TZP basis sets were used with triple-ξ-accuracy sets of Slater-type orbitals, with polarization functions added to all atoms. Relativistic corrections were made using the ZORA (zero-order relativistic approximation) formalism,[35] and the core electrons were frozen up to 1s for C, N, O and F; 2p for P and Cl; 3d for Rh and Pd; and 4d for Ir and Pt. The local density approximation of Vosko, Wilk, and Nusair[36] was utilized. All quoted electronic structure data from optimized structures use an integration grid of 6.0 and were verified as minima using frequency calculations. Fragment analyses use the MOs of the chosen fragments as the basis set for the molecular calculation. Initial spin-restricted calculations are carried out on the fragments with the geometry that they have in the molecule; thus the fragments are in a prepared singlet state. Neutral fragments were chosen, as this assisted in drawing up the MO diagrams. Topological analyses of the electron density were performed using the XAIM program.[37] The *adf2aim* executable, which is provided with the standard source code of the ADF program, was used to convert the tape21 file to a wave function (.wfn) file. XAIM was then used to locate and characterize the critical points.

Synthesis and Characterization of New Compounds. [(2-Phenylpyridine)Pd(TFA)]$_2$ (3). $Pd(TFA)_2$ (0.50 g, 1.50 mmol) was added to a three-neck 250 mL round-bottom flask equipped with a reflux condenser and a stir bar. Chloroform (80 mL, Omnisolv) and 2-phenylpyridine (0.233 g, 1.50 mmol) were added, and the solution was heated for 5 h at reflux. The yellow solution was allowed to cool and was filtered through Celite to remove any palladium black. The solvent was removed in vacuo to give a brown oil. The crude product was purified using column chromatography (eluting first with CH_2Cl_2 and then ethyl acetate) to give [(2-phenylpyridine)Pd(TFA)]$_2$ (**3**) as a yellow powder (0.24 g, 48%). X-ray diffraction quality crystals were grown from saturated solutions of CH_2Cl_2 or acetone. ^{1}H NMR (300 MHz, chloroform-d_1): δ 7.75 (m, 2H), 7.47 (app td, J = 7.5, 0.9, 2H), 7.15 (d, J = 8.2, 2H), 6.86 (m, 6H), 6.74 (m, 2H), 6.58 (app t, J = 6.4, 2H). ^{13}C{^{1}H} NMR (125 MHz, chloroform-d_1): δ 164.3 (2C), 149.8 (2C), 148.6 (2C), 144.3 (2C), 138.5 (2C), 132.1 (2C), 131.0 (2C), 129.1 (2C), 125.0 (2C), 122.9 (2C), 121.9 (2C), 121.6 (2C), 117.8 (2C). HRMS for $[C_{26}H_{16}F_6N_2O_4Pd_2]^+$, calcd: 747.9100 g/mol. Found: 747.9135 g/mol.

[(2-*p*-Tolylpyridine)Pd(TFA)]$_2$ (4). The above procedure was followed, substituting 2-*p*-tolylpyridine (0.255 g, 1.50 mmol), to give [(2-*p*-tolylpyridine)Pd(TFA)]$_2$ (**4**) as a yellow powder (0.21 g, 36%). X-ray diffraction quality crystals were grown from a saturated solution of CH_2Cl_2. ^{1}H NMR (300 MHz, dichloromethane-d_2): δ 7.69 (m, 2H), 7.47 (app td, J = 7.8, 1.5, 2H), 7.11 (d, J = 8.1, 2H), 6.80 (m, 4H), 6.63 (m, 4H), 2.16 (s, 6H). ^{13}C{^{1}H}NMR (125 MHz, dichloromethane-d_2): δ 164.8 (2C), 149.6 (2C), 148.7 (2C) 141.2 (2C), 136.5 (2C), 132.4 (2C), 131.6 (2C), 131.0 (2C), 126.3 (2C), 123.3 (2C), 122.5 (2C), 121.4 (2C), 118.3 (2C), 23.2 (4C). HRMS for $[C_{28}H_{20}F_6N_2O_4Pd_2]^+$, calcd: 775.9414 g/mol. Found: 775.9418 g/mol.

Acknowledgment. We thank George Rossman and Elizabeth Miura Boyd for assistance with single-crystal Raman spectroscopy and Larry Henling and Michael Day for assistance with X-ray crystallography. This work was supported by BP through the MC^2 program, the NSF Center for Chemical Innovation (Powering the Planet, CHE-0802907 and CHE-0947829), and CCSER (Gordon and Betty Moore Foundation). The Bruker KAPPA APEXII X-ray diffractometer used in this work was purchased via an NSF CRIF:MU CHE-0639094 award to the California Institute of Technology.

Supporting Information Available: X-ray crystallographic files in CIF format for the structure determinations of **1**−**6** and further details of the electrochemistry, photophysics, and DFT calculations. This material is available free of charge via the Internet at http://pubs.acs.org.

(34) (a) Fonseca Guerra, C.; Snijder, J. G.; Te Velde, G.; Baerends, E. J. *Theor. Chem. Acc.* **1998**, *99*, 391. (b) Te Velde, G.; Bickelhaupt, F. M.; Baerends, E. J.; Fonseca Guerra, C.; Van Gisbergen, S. J. A.; Snijders, J. G.; Ziegler, T. *J. Comput. Chem.* **2001**, *22*, 931. (c) *ADF2007.01*; SCM, Theoretical Chemistry, Vrije Universiteit: Amsterdam, The Netherlands. http://www.scm.com (accessed Jan 2010).

(35) (a) Vanlenthe, E.; Baerends, E. J.; Snijders, J. G. *J. Chem. Phys.* **1993**, *99*, 4597. (b) Vanlenthe, E.; Baerends, E. J.; Snijders, J. G. *J. Chem. Phys.* **1994**, *101*, 9783. (c) Vanlenthe, E.; Baerends, E. J.; Snijders, J. G. *J. Chem. Phys.* **1996**, *105*, 6505. (d) Vanlenthe, E.; Ehlers, A.; Baerends, E. J. *J. Chem. Phys.* **1999**, *110*, 8943. (e) Vanlenthe, E.; VanLeeuwen, R.; Baerends, E. J.; Snijders, J. G. *Int. J. Quantum Chem.* **1996**, *57*, 281.

(36) Vosko, S. H.; Wilk, L.; Nusair, M. *Can. J. Phys.* **1980**, *58*, 1200.

(37) Alba, J. C. O.; Jané, C. B. *XAim*; Universitat Rovira i Virgili: Tarragona Spain, **1998** (download free of charge from the Web distribution site: http://www.quimica.urv.es/XAIM/, accessed Jan 2010).